university of groningen

KATHOLIEKE UNIVERSITEIT LEUVEN

Spin Crossover in $Fe^{II}(L)_n(NCS)_2$ Complexes:

A CASPT2 study

Master Thesis

European Master in Theoretical Chemistry and Computational Modelling
TCCM 2010-2012

Daniel Sethio

Supervisors: dr. Steven Vancoillie
dr. Remco W. A. Havenith
prof. dr. Kristine Pierloot
prof. dr. Ria Broer

Master Thesis presented in fulfillment of the requirements for the degree of Master of Chemical Physics

Academic year 2010-2012

Abstract

High-level *ab initio* calculations using the CASPT2 method and extensive basis sets have been performed on two $3d^6$ pseudo-octahedral $Fe^{II}(L)_n(NCS)_2$ complexes, $Fe(NCH)_4(NCS)_2$ and $Fe(bpy)_2(NCS)_2$. The structural properties that change during spin crossover processes, the High Spin-Low Spin energy differences, and potential energy profiles were studied. The validation of the method was performed on the model complex, $Fe(NCH)_4(NCS)_2$. Several active spaces, basis sets, and geometries were considered. The CASPT2[10,12] procedure, with CASSCF active spaces consisting of two σ ligands orbitals with e_g symmetry, five Fe-3d orbitals, and five Fe-3d$'$ orbitals, with medium-sized basis set is considered as an adequate method. For geometry optimization, a hybrid CASPT2/PBE0 method (the metal-ligand distance is optimized at CASPT2 level while the rest of molecule is optimized at PBE0 level) is recommended as an inexpensive alternative to obtain geometries close to the fully CASPT2 geometry.

Samenvatting

Er zijn nauwkeurige *ab initio* berekeningen, gebruikmakend van de CASPT2 methode en uitgebreide basissets, uitgevoerd voor twee $3d^6$ pseudo-octahedrale $Fe^{II}(L)_n(NCS)_2$ complexen, namelijk $Fe(NCH)_4(NCS)_2$ en $Fe(bpy)_2(NCS)_2$. De structuureigenschappen die veranderen tijdens spin crossover processen, de Hoog Spin-Laag Spin energieverschillen, en de potentiële energieprofielen werden bestudeerd. Het modelcomplex $Fe(NCH)_4(NCS)_2$ werd gebruikt ter validatie van de methode. Verscheidene actieve ruimtes, basissets en geometrieën werden in beschouwing genomen. De CASPT2[10,12] procedure, waarbij de CASSCF actieve orbital ruimte bestaat uit twee σ ligand orbitalen met e_g symmetrie, vijf Fe-3d orbitalen en vijf Fe-3d′ orbitalen, met een middelgrote basisset wordt aangemerkt als een geschikte methode. Voor geometrie optimalisaties wordt een gemengde CASPT2/PBE0 methode aanbevolen, waarbij de metaal-ligand afstand wordt geoptimaliseerd op CASPT2 niveau terwijl de rest van het molecuul wordt geoptimaliseerd op PBE0 niveau, als een goedkoop alternatief om geometrieën te krijgen die overeenkomen met de volledige CASPT2 geometrie.

Contents

Introduction

Molecular magnetism is a new class of fascinating materials. These molecules exhibit a finite number of interacting spin centers and provide ideal opportunities to study fundamental concepts of magnetism. The spin crossover (SCO) is one type of molecular magnetism where the spin state and magnetic moment of the transition metal complexes can be changed or controlled by external constraints. The spin crossover processes are accompanied by the structural change.

In order to understand the nature and the mechanism of SCO, it is necessary to investigate the difference in molecular geometry between the two states. The occurring spin transition (ST) influences the structure of the compounds, especially the metal-ligand bond distances, which are very sensitive to the spin states. In the family of FeN_6 pseudo-octahedral complexes, the Fe-N bond distances change by about 0.2 Å [1], the Fe-N bond distances being longer in the HS state and shorter in the LS state. Moving the electrons from the $t_{2g}(O_h)$ to the $e_g(O_h)$ orbital causes an increase of the electron repulsion, resulting in longer Fe-N bonds. This lengthening of Fe-N bonds make the ligand field strength weaker and as a consequence the HS state becomes energetically more preferable.

To study the relationship between the spin crossover and the structural properties, we took one of the compounds in the family of $Fe^{II}(L)_n(NCS)_2$, namely $Fe(bpy)_2(NCS)_2$ [2] (bpy = bipyridine) (Figure 1b). The complex is a thermally active SCO compound [3]. However, the size of this complex prohibits it to be used for finding a suitable computational procedure with sufficient accuracy. Therefore, the $Fe(NCH)_4(NCS)_2$ (Figure 1a) was used as a hypothetical model [4] for $Fe(bpy)_2(NCS)_2$, where two bidentate bpy ligands are replaced by four monodentate NCH ligands. After validating the method used for the model, the same method was used to describe the target compound for which the spin crossover phenomenon is observed. In this work, we will focus on studying the structural properties that change during the spin crossover processes, the ST energy difference, and the potential energy profiles.

The thesis is organized in four chapters. Chapter one starts with an introduction to

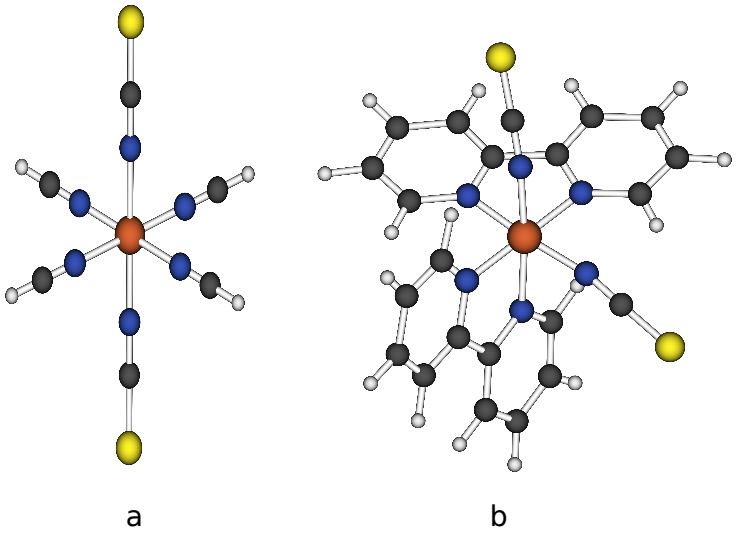

Figure 1: Spin crosser complexes: (a). The model system $Fe(NCH)_4(NCS)_2$ (b). The real system $Fe(bpy)_2(NCS)_2$

SCO, followed by rationalization of the spin crossover phenomenon by ligand field theory [3]. In addition, the multiconfigurational second order perturbation theory (CASPT2) and density functional theory are briefly described. The methodologies that are being used in the investigation are discussed in chapter two. Results on both the hypothetical method, $Fe(NCH)_4(NCS)_2$ complex, and the real system, $Febpy_2(NCS)_2$ complex, are presented in chapter three. Finally, the thesis ends with conclusions and an outlook for some possible future investigations.

Chapter 1

Theoretical Background

1.1 Introduction to Spin Crossover

Spin crossover (SCO) is a phenomenon, in which the spin state of some transition metal compounds can change between two states: low spin (LS) and high spin (HS). The interchange between two states, LS and HS, can be induced by external stimuli such as changing the temperature (thermal spin-crossover), changing the pressure, changing the solvent, applying magnetic field, or by irradiation with light (light-induced excited state spin trapping, LIESST) (Figure 1.1) [5,6].

The spin crossover phenomenon was discovered for the first time by Cambi and coworkers in a synthetic compound in the 1930s [7]. The interconversion of two spin states as a result of variation in temperature was observed in Fe(III) dithiocarbamate derivatives. Besides in synthetic systems, spin transitions are also found in natural systems. In nature, the ST plays an important role in the chemical reactivity of biological systems, such as metalloenzymes, e.g., the catalytic cycle of cytochrome P450 [8] and some of haem derivatives, e.g., haemoglobin [9]. The structural switch of haemoglobin between its active and inactive form is strongly coupled with the LS-HS spin transition in response to the

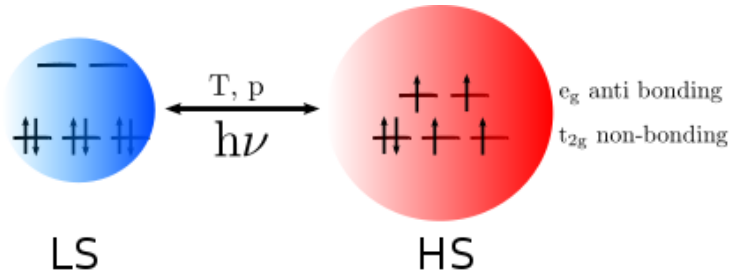

Figure 1.1: Schematic description of the spin crossover process for a transition metal-$3d^6$ system. The spin transition between two states can be induced by temperature, pressure, and light. (adapted from Ref. [4])

oxygenation-deoxigenation process [10, 11].

SCO complexes are intensively investigated due to their highly potential as candidates in electronic materials. The SCO compounds have been proposed for some applications, such as a thermal sensor, optical switch, memory, and data storage devices [1, 12]. Recently, the SCO compounds are proposed to be used as dye-sensitizers in dye-sensitized solar cells [13].

The SCO phenomenon is observed in some transition metal compounds with a d^4 to d^7 electronic configuration in an octahedral ligand field. The family of quasi-octahedral compounds of Fe(II) is the best known and the largest number of the active spin-crossover compounds [3, 14]. This family presents an important class of switchable molecular systems [15]. The electronic structure of Fe(II) complexes will be explained in the following section (Sec. 1.2).

1.2 Ligand Field Theory

In the octahedral crystal field, the five-3d orbitals of the transition metal ion are split into lower-energy triply degenerate t_{2g} orbitals, namely d_{xy}, d_{yz} and d_{xz}, and higher-energy doubly degenerate e_g orbitals, namely d_{z^2} and $d_{x^2-y^2}$ (Figure 1.2). The electrons in the d_{z^2} and $d_{x^2-y^2}$ (e_g) orbitals are concentrated along the axes whereas the electrons in the d_{xy}, d_{yz} and d_{xz} (t_{2g}) orbitals are concentrated in regions that lie between the ligands (Figure 1.3). In ligand field theory, the six ligands are represented as six point negative charges in an octahedral array around the central metal ion. The electrons in the e_g orbitals are repelled more strongly by the negative charge on the ligands than the electrons in the t_{2g} orbitals. As a result, the two degenerate e_g orbitals lie above the three degenerate t_{2g} orbitals [16]. The splitting between the two sets, t_{2g} and e_g orbitals, is called ligand-field splitting, Δ_o or 10Dq.

The ligand-field splitting Δ_o depends on the ligand field strength and the metal-ligand distance as $1/r^n$, with n=5-6 [3]. Shorter metal-ligand distances increase Δ_o, whereas longer metal-ligand distances decrease Δ_o. In the case of the iron(II) complexes, the iron(II) center has the valence electronic configuration $3d^6$(Figure 1.1). In strong fields, the electrons occupy the lower t_{2g} orbitals (t_{2g}^6, $^1A_1$, low spin, large Δ_o) while in weak fields, they occupy both t_{2g} and e_g orbitals ($t_{2g}^4e_g^2$, $^5T_{2g}$, high spin, small Δ_o). The spin state of iron(II) can change from diamagnetic (S=0) in the LS state to paramagnetic (S=2) in the HS state.

The nature of the spin states of the SCO complexes originated from the competition between the pairing energy of the electrons in the valence d orbitals (Π) and ligand-field splitting (Δ_o) [3, 14]. In the situation where the spin-pairing energy is larger than Δ_o, the HS state is favored. If the spin-pairing energy is smaller than Δ_o, the LS state is favored.

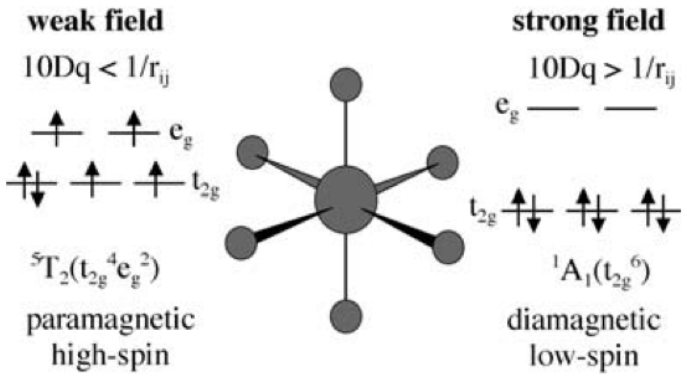

Figure 1.2: The electronic configurations of the two possible ground states for iron(II) in an octahedral crystal field.
(taken from Ref. [3])

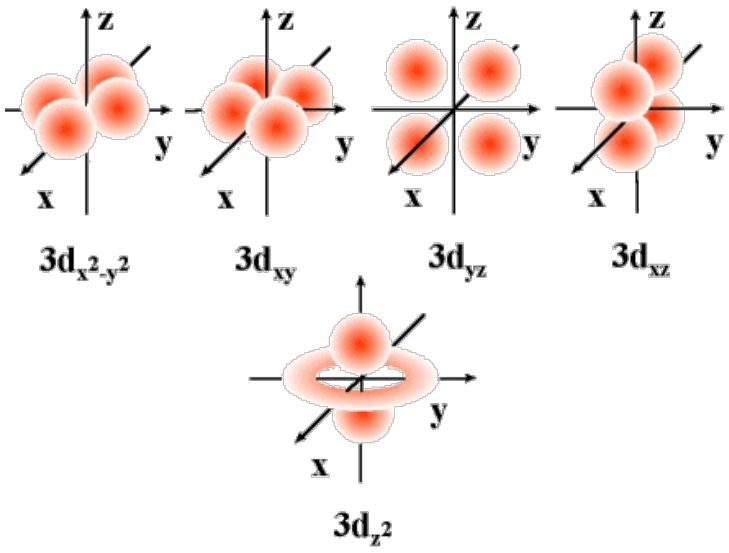

Figure 1.3: The five d orbitals: $d_{x^2-y^2}$, d_{xy}, d_{yz}, d_{xz}, and d_{z^2}.
(taken from http://www.mikeblaber.org/oldwine/chm1045/notes/Struct/Orbitals/Struct06.htm)

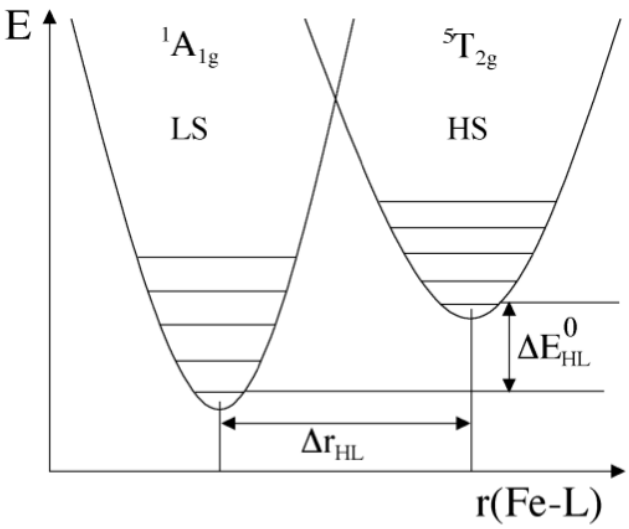

Figure 1.4: Adiabatic potentials for the HS and LS state along the most important reaction coordinate, the breathing mode, for spin crossover, namely the totally symmetry metal-ligand stretch vibration denoted r(Fe-L).
(taken from Ref. [3])

The energy difference between HS and LS, denoted as $\Delta E_{HL}(\Delta E_{HL} = E_{HS} - E_{LS})$, is a key parameter for determining the spin transition [14]. Thermodynamically, the condition for the phenomenon of a thermal spin crossover to occur, ΔE_{HL} should be of the order of thermally accessible energies, k_BT (Figure 1.4). At very low temperature, the complexes should be in LS state, whereas at higher temperature the HS state is populated entropy-driven [3]. It was shown experimentally that the active thermal spin-crossover compounds exhibit a ΔE_{HL} in the order of 0-2000 cm^{-1} [3, 5], e.g., ΔE_{HL} of the $Fe(bpy)_2(NCS)_2$ complex is 844 cm^{-1} [17]. For a ΔE_{HL} larger than 2000 cm^{-1}, the SCO is difficult to reach thermally. It is found that for the $Fe(II)(bpy)_3^{2+}$ complex ($\Delta E_{HL} \approx 6000$ cm^{-1}) [18], the spin transition can be reached optically (LIESST).

1.3 Multiconfigurational Second Order Perturbation Theory

The multiconfigurational second order perturbation theory (MRPT2) is a standard scheme to account for dynamic and non-dynamic correlations in the case of the multiconfigurational wave functions of medium- to large-sized systems [4]. The complete active space second order theory (CASPT2) is one of the most widely used MRPT2 methods [19]. CASPT2 is constructed by applying second-order perturbation theory on a complete active space self consistent field (CASSCF) wave function as a reference. The CASSCF wave function is obtained by performing a full configuration interaction (FCI) in a limited ac-

tive space and simultaneously optimizing both CI and all occupied and active orbital expansion coefficients.

The idea of CASPT2 method is simple: to compute the second-order energy with a CASSCF wave function as the zeroth-order approximation. The approximate zeroth-order Hamiltonian $\hat{H}^{(0)}$ and reference (root) function $\Psi^{(0)}$ should satisfying

$$\hat{H}^{(0)}\Psi^{(0)} = E_0\Psi^{(0)} \tag{1.1}$$

where E_0 is the eigenvalue of $\Psi^{(0)}$.

The reference wave function

The reference wave function in CASPT2 method is a CASSCF wave function. The CASSCF wave function is obtained by performing a full CI in a limited active space. In the full configurational interaction (FCI) method, the wave function is constructed by including all possible excitations

$$\Psi^{(0)} = c_0\Phi_0 + \sum_{a,i} c_a^i\Phi_a^i + \sum_{\substack{a<b\\i<j}} c_{ab}^{ij}\Phi_{ab}^{ij} + \sum_{\substack{a<b<c\\i<j<k}} c_{abc}^{ijk}\Phi_{abc}^{ijk} + ... \tag{1.2}$$

where c_0, c_a^i, c_{ab}^{ij}, and c_{abc}^{ijk} are expansion coefficient of ground state, singly, doubly, and triply excited configurations, respectively, while Φ_0, Φ_a^i, Φ_{ab}^{ij}, and Φ_{abc}^{ijk} are ground state, singly, doubly, and triply excited determinant, respectively. The ground state HF determinant is used for the Φ_0.

The FCI approach is an exact method within the chosen one electron basis. However, this approach is highly demanding on computer resources. This method is mainly used in accurate studies of small molecules. For larger systems, the number of configurations is being restricted, which is the basis idea of the multiconfigurational self-consistent field (MCSCF) method. The MCSCF wave function is a truncated CI expansion

$$\Psi_{MCSCF} = \sum_I c_I|\Psi_I\rangle \tag{1.3}$$

in which both the CI expansion coefficient c_I and the orbital coefficients in the configuration state functions (CSF) $|\Psi_I\rangle$ are simultaneously optimized governed by variational principle. CSF is the smallest expansion in the term of Slater determinant (SD), that obey the spin- and symmetry requirement for a wave function.

In a CASSCF wave function, the molecular orbital space consists of three different subspaces: inactive, active, and external. The inactive orbitals are assumed to be doubly occupied in all CSFs while the external orbitals are assumed to be unoccupied in all CSFs. The remaining active orbitals consist of occupied and virtual orbitals which are carefully selected. Selecting the 'correct' active spaces need some 'experimenting' with different

choices of active spaces in order to asses the adequacy and convergence behavior [19]. In the case of Fe(II) compounds, it is necessary to account for the double-shell effect (extra d-shell) [20].

The Zeroth-order Hamiltonian

For the multiconfigurational case, the zeroth-order Hamiltonian is chosen as:

$$\hat{H}^{(0)} = \hat{P}_0\hat{F}\hat{P}_0 + \hat{P}_K\hat{F}\hat{P}_K + \hat{P}_{SD}\hat{F}\hat{P}_{SD} + \hat{P}_X\hat{F}\hat{P}_X \tag{1.4}$$

where $\hat{\mathrm{P}}$ and $\hat{\mathrm{F}}$ are the projection and the Fock operator, respectively. The CI space is partitioned into four different subspaces: 0 refers to the reference (root) function, K refers to the rest of CAS CI space, SD refers to the all singly and doubly excited CSFs with respect the CAS reference, and X refers to the rest of CI space.

The generalized Fock matrix is assumed as a summation of one-electron operators:

$$\hat{F} = \sum_{p,q} f_{pq}\hat{E}_{pq} \tag{1.5}$$

where

$$f_{pq} = h_{pq} + \sum_{r,s} D_{rs}[(pq|rs) - \frac{1}{2}(pr|qs)] \tag{1.6}$$

The f_{pq} corresponds to the matrix element for molecular orbitals ψ_p, ψ_q and $\hat{\mathrm{E}}_{pq}$ corresponds to the conventional spin-summed excitation operator in second quantization. The orbital indices are denoted *i, j, k, l* for inactive orbitals, *t, u, v, x* for active orbitals, and *p, q, r, s* in the absence of any specification.

The CASPT2 wave function

The dynamical correlation is obtained by using second order perturbation theory on a CASSCF reference wave function. The second-order energy correction is obtained from:

$$E_2 = \langle\Psi_0|\hat{H}_1|\Psi_1\rangle \tag{1.7}$$

where Ψ_1 is built from two-electron excitations from the root function.

$$\Psi_1 = \sum_{pqrs} C_{pqrs}\hat{E}_{pq}\hat{E}_{rs}\Psi_0 \tag{1.8}$$

Nowadays, the multiconfigurational perturbation theory (CASPT2) is the gold standard method to treat nearly degenerate between different electronic configurations [21]. The CASPT2 method is the accurate method in widely applications, particularly in electronic spectroscopy [22].

1.4 Density Functional Theory

The basic idea of density functional theory (DFT) is to relate the total ground-state energy of a system to its ground-state density $E \Leftrightarrow \rho(\vec{r})$. The ground-state electronic energy of an n-electron system can be expressed as

$$E[\rho] = -\frac{1}{2}\sum_{i=1}^{n}\int \psi_i^*(\vec{r_1})\nabla_i^2\psi_i^*(\vec{r_1})d(\vec{r_1}) - \sum_{x=1}^{N}\int \frac{Z_x}{r_{xi}}\rho(\vec{r_1})d(\vec{r_1}) + \frac{1}{2}\iint \frac{\rho(\vec{r_1})\rho(\vec{r_2})}{|(\vec{r_1}) - (\vec{r_2})|}d(\vec{r_1})(\vec{r_2}) + E_{XC}[\rho] \tag{1.9}$$

where ψ_i's are the Kohn-Sham orbitals, the first term correspond to the kinetic energy of non-interacting electrons, the second term represents the nuclear-electron interaction, the third term refers to Coulombic repulsions between two electron densities, and the fourth is exchange-correlation term, represents the correction to the kinetic energy arising from the interacting nature of electrons and all non-classical correction to the electron repulsion energy [23]. The ground-state electron density $\rho(r)$ can be expressed as a sum of densities of a set of one-electron Kohn-Sham orbitals:

$$\rho(r) = \sum_{i=1}^{n}|\psi_i(r)|^2 \tag{1.10}$$

The Kohn-Sham orbitals are obtained by solving the Kohn-Sham equation which can be obtained by applying the variational principle to the electronic energy $E[\rho]$.

$$\hat{h}_i\psi_i(r_1) = \varepsilon_i\psi_i(r_1) \tag{1.11}$$

where $\hat{h}_i$ and ε_i correspond to the Kohn-Sham Hamiltonian and the Kohn-Sham orbital energy, respectively. The Kohn-Sham Hamiltonian can be expressed as

$$\hat{h}_i = -\frac{1}{2}\nabla_1^2 - \sum_{x=1}^{N}\frac{Z_x}{\vec{r_{xi}}} + \int \frac{\rho\vec{r_2}}{|\vec{r_1} - \vec{r_2}|}d\vec{r_2} + V_{XC}[\vec{r_1}] \tag{1.12}$$

where V_{XC} refers to the functional derivative of the exchange-correlation energy which is given by

$$V_{XC}[\rho] = \frac{\delta E_{XC}[\rho]}{\delta\rho} \tag{1.13}$$

The Kohn-Sham equation is solved in a self-consistent method, starting from a guess charge density ρ which is a superposition of atomic densities. The V_{XC} is calculated by using an approximate E_{XC}, yielding an initial set of Kohn-Sham orbitals. A new density is obtained from this set of Kohn-Sham orbitals (Equation 1.10). This process is repeated until the density and exchange-correlation energy have fulfilled a chosen convergence criterion. After the convergence criterion was satisfied, the electronic energy is computed by 1.9 [23].

Equation 1.9 must be solved approximately because the exact exchange-correlation (xc) functional is unknown. If the exact E_{XC} were known, these equations would have produced the exact total energy and density. Several approximations have been proposed:

Local Density Approximation (LDA)

The simplest approach to represent the exchange-correlation functional is the local density approximation (LDA). In LDA, it is assumed that the exchange-correlation energy at any point in space is a function of electron density at that point in space only and can be specified by the electron density of a homogeneous electron gas of the similar density. In 1930, Dirac proposed local density approximation for the first time as

$$E_{XC}^{LDA}[\rho] = \int \rho(\vec{r})\varepsilon_{xc}^{ueg}[\rho(\vec{r})]d\vec{r} \tag{1.14}$$

where $\varepsilon_{xc}^{ueg}[\rho(\vec{r})]$ is the exchange-correlation energy per particle of the uniform electron gas which can be split into contributions from exchange and correlation as shown as

$$\varepsilon_{xc}^{ueg}[\rho(\vec{r})] = \varepsilon_{x}^{ueg}[\rho(\vec{r})] + \varepsilon_{c}^{ueg}[\rho(\vec{r})] \tag{1.15}$$

where the exchange energy can be specified as

$$\varepsilon_{xc}^{ueg}[\rho(\vec{r})] = -\frac{3}{4}\left(\frac{3}{\pi}\right)^{1/3}\rho^{4/3}(\vec{r})d\vec{r} \tag{1.16}$$

The correlation energy ε_c per particle is hardly to obtain separately from the exchange energy. Usually this is obtained by a suitable interpolation formula, starting from a set of values calculated for a number of different densities in a homogeneous electron gas [23].

Although its conceptual simplicity, the LDA approximation is surprisingly accurate, despite some typical deficiencies, such as the adequate cancellation of self-interaction contributions. In particular, LDA usually yields an underestimation to the atomic ground-state energies and ionization energies, while binding energies are typically overestimated.

Local Spin Density Approximation (LSDA)

The local spin density approximation (LSDA) accounts for spin dependence into functionals. The LSDA is devised to solve several conceptual problems of LDA that are subjected to an external magnetic field, polarized system, and relativistic effects. The exchange functional in LSDA is specified by

$$\varepsilon_{x}^{LSDA}[\rho] = 2^{1/3}\frac{3}{4}\left(\frac{3}{\pi}\right)^{1/3}\int(\rho_{\alpha}^{4/3} + \rho_{\beta}^{4/3})d\vec{r} \tag{1.17}$$

where ρ_α and ρ_β are spin up, spin down densities, respectively. For closed-shell systems, ρ_α and ρ_β are equal, and LSDA becomes identical to LDA. It is also recognized to overly favor high spin-state structures. In general LDA is worse for small molecules, improving with the size of the system.

Generalized Gradient Approximation (GGA)

A homogeneous electron gas are commonly very different from molecular systems. In reality, any real system is spatially inhomogeneous; it has a spatially varying density. This effect is accounted in generalized gradient approximation methods (GGA) by making the exchange and correlation energies dependent not only on the density but also on the gradient of the density $\nabla\rho(r)$.

$$E_{GGA}^{XC}[\rho] = \int \varepsilon_{XC}(\rho, |\nabla\rho|, \nabla^2\rho)d\vec{r} \tag{1.18}$$

Generally, GGA methods improve significantly compare to the LDA methods. GGA methods give a better results for total energies, atomization energies, structural energy differences, and energy barriers. GGA methods usually give reliable results for covalent, ionic, metallic, and hydrogen bonds, however they fail for van der Waals interactions [24, 25]. In the solid state, GGA functionals do not yield significantly better results than LDA, nor in the calculation of ionization potentials and electron affinities [26–28].

The next step in improvement of gradient approximations is called meta-GGA. Meta-GGA was developed by including additional semilocal information beyond the first-order density gradient contained in GGA. These methods depend explicitly on higher order density gradients or typically on the kinetic energy density, which involves derivatives of the occupied Kohn-Sham orbitals. Meta-GGA methods give a significant improvement in determination of properties such as atomization energies.

Hybrid Density Functionals

Hybrid density functional methods combine the exchange-correlation of GGA method with a certain percentage of Hartree-Fock exchange.

$$E_{Hybrid}^{XC} = E_c + \alpha E_x^{HF} \tag{1.19}$$

where α is percentage of Hartree-Fock exchange. A certain degree of empiricism is used in optimizing the weight factor for each component and the functionals that are mixed. In the case of PBE0 functional, this functional contains 25% HF exchange [29].

Hybrid functionals represent a significant improvement over GGA for many molecular properties. Hybrid density functional methods have become a very popular choice in quantum chemistry and are now widely used. In solid-state physics this type of functional was much less successful due to difficulties in computing the exact-exchange part within a plane-wave basis set, i.e., B3LYP [30–32].

Chapter 2

Methods

Symmetry was enforced during the calculations. The $Fe(NCH)_4(NCS)_2$ complex has D_{4h} symmetry while $Fe(bpy)_2(NCS)_2$ has C_2 symmetry. Some limitations of the software to make use of symmetry cause the pseudo-octahedral complexes to be treated in the D_{4h} or D_{2h} point group for $Fe(NCH)_4(NCS)_2$. Figure 2.1 shows the correlation between the different point groups. In O_h symmetry, the five 3d orbitals of the transition metal split into t_{2g} and e_g. In D_{4h} symmetry, the $t_{2g}(O_h)$ reduces to $b_{2g} \oplus e_g$ whereas $e_g(O_h)$ reduces to $a_{1g} \oplus b_{1g}$. In D_{2h} symmetry, the irreducible representation of D_{4h} point group, b_{2g} reduces to b_{1g}, e_g to $b_{2g} \oplus b_{3g}$, a_{1g} to a_g, and b_{1g} to a_g. Furthermore in C_2 symmetry, b_{1g} and a_g of the D_{2h} point group reduces to a, while the b_{2g} and b_{3g} reduce to b [33].

The geometry optimizations were performed for two different spin states: singlet and quintet. To study the structural properties of the SCO compounds, the geometry optimizations were performed at three different levels of theory: fully optimized at DFT(PBE0) level, optimized metal-ligand distances at CASPT2 level and the rest at DFT level (CASPT2/PBE0), and fully optimized at CASPT2 level.

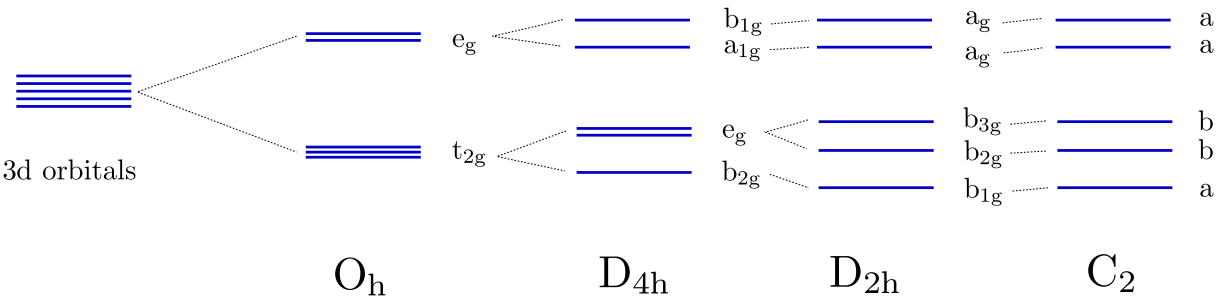

Figure 2.1: Schematic correlation table between the irreducible representations in the O_h, D_{4h}, D_{2h}, and C_2 point group.

2.1 Optimization at DFT level

All DFT calculations were performed using TURBOMOLE V6.3 [34]. All calculations were performed in D_{4h} and D_{2h} symmetry. The calculations were performed using the PBE0 functional using the def2-TZVP basis set. This basis set give reasonable geometries with inexpensive computational costs.

The PBE0 functional has been shown to be the most adequate for giving reasonable structures for transition metal complexes [35]. As is shown in Ref. [35], the Hartree-Fock (HF) method tends to overestimate Fe-L distances, while the local DFT method tends to underestimate Fe-L distances. By mixing 25% of HF exchange into the PBE0 functional seems to give a reasonable structure. PBE0 functional with def2-TZVP give a reasonable structures for transition metal complexes.

The geometry optimizations were performed for the closed-shell singlet state, corresponding to the $^1A_{1g}(b_{2g}^2e_g^4)$ state in D_{4h}. In order to find the lowest-energy quintet configuration and to see if the excited states was Jahn-Teller active, the different electronic configurations were calculated (Figure 3.1). A Jahn-Teller distorted structure was checked by further lowering the symmetry to D_{2h}. Five different electronic configurations were studied: two configurations belong to the D_{4h} point group and three others configurations belong to the D_{2h} point group. Two configurations in D_{4h} point group correspond to $^5B_{1g}(b_{2g}^2e_g^2a_{1g}^1b_{1g}^1)$ and $^5E_g(b_{2g}^1e_g^3a_{1g}^1b_{1g}^1)$. Three configurations in D_{2h} correspond to $^5B_{1g}(b_{1g}^2b_{3g}^1b_{2g}^1a_g^1a_g^1)$, $^5B_{2g}(b_{1g}^1b_{3g}^1b_{2g}^2a_g^1a_g^1)$, and $^5B_{3g}(b_{1g}^1b_{3g}^2b_{2g}^1a_g^1a_g^1)$.

On the PBE0 optimized geometries of the lowest quintet $^5B_{1g}(b_{2g}^2e_g^2a_{1g}^1b_{1g}^1)$ and the singlet $^1A_{1g}(b_{2g}^2e_g^4)$ state were followed by single point CASPT2 calculations.

2.2 Optimization at CASPT2 level

The CASSCF/CASPT2 calculations were performed using MOLCAS 7.6 [36, 37]. The scalar relativistic effects were included using a second order Douglas-Kroll-Hess (DKH) Hamiltonian [38, 39]. All CASPT2 calculations were performed using atomic natural orbital (ANO)-type basis sets, in particularly the ANO-rcc basis set [40]. This basis set is designed to include relativistic effects and to provide an improved description of semi core correlation. In basis I, the Fe ANO-rcc basis set, contracted to [7s6p5d2f1g] was combined with ANO-rcc basis sets for other atoms, contracted to [4s3p1d] for O and N, contracted to [5s4p2d] for S, and contracted to [2s1p] for H. In basis II, the Fe ANO-rcc basis set, contracted to [7s6p5d3f2g1h], was combined with ANO-rcc-type basis sets for other atoms, contracted to [4s3p2d1f] for N and C atoms, contracted to [5s4p2d1f] for S atoms, and contracted to [3s1p] for H atoms. In basis III, the Fe ANO-rcc basis set, contracted to [10s9p8d6f4g2h], was combined with ANO-rcc-type basis sets for other atoms, contracted to [8s7p4d3f2g] for N and C atoms, contracted to [8s7p5d4f2g] for S

atoms, and contracted to [6s4p3d1f] for H atoms.

In order to know the information about the importance and the source of non-dynamical correlation effects, we increased the active space gradually. Four different active spaces were used to obtain the CASSCF wave function. The CASSCF wave function is constructed by performing a full configuration interaction (FCI) in a limited active space and simultaneously optimizing both the CI and orbital expansion coefficients. The CAS[10,10] is considered as minimum active space to capture the essential correlation effects. In CAS[10,10], the active space consists of the five Fe-3d, two bonding ligand σ orbitals of e_g symmetry, and three orbitals Fe-3d′ of t_{2g} symmetry (Figure 2.2). In CAS[10,12], the active space consists of the five Fe-3d, two bonding ligand of e_g symmetry to describe non-dynamic correlation effects associated with covalent metal-ligand interactions, and five Fe-3d′ to describe the so-called double-shell effect [41]. This active space ensures the balanced description of the dynamical correlation associated with the Fe-3d electrons [42,43] and non-dynamical correlation effects associated with the covalent metal-ligand interactions [35,41,44]. In CAS[10,13], the active space consists of the five Fe-3d, two bonding ligand of e_g symmetry, three orbitals Fe-3d′ of t_{2g} symmetry, and three ligand π^* orbitals. In CAS[10,15], the active space consists of the five Fe-3d, two bonding ligand of e_g symmetry, five orbitals Fe-3d′ of t_{2g} symmetry, and three ligand π^* orbitals [18].

For the singlet state, ten electrons are distributed in two types of orbitals: six electrons occupying t_{2g} orbital and four electrons occupying two bonding ligand e_g symmetry. For the quintet state, ten electrons are distributed in three types of orbitals: four electrons occupying t_{2g} orbital, two electrons occupying e_g orbital, and four electrons occupying two bonding ligand e_g symmetry. In all CASPT2 calculations the core electrons, i.e., from N,C, S, and H, 1s and Fe 1s-2p were kept frozen. All CASPT2 calculations were performed using an imaginary level shift of 0.1 and an IPEA shift 0.25 to avoid intruder states and to provide a balanced description of open and closed shells [45,46].

2.3 Optimized metal-ligand bond distances at CASPT2 level and the reminder at PBE0 level (CASPT2/PBE0)

The equilibrium structures for the HS and the LS states were obtained by a series of point calculations for the two states. A series of structures was first obtained from a partial optimization with PBE0, fixing only the metal-ligand distances at a certain value. After performing single-point CASPT2 calculations on each of these structures, the optimal metal-ligand distances at the CASPT2 level were obtained from a quadratic fitting [35].

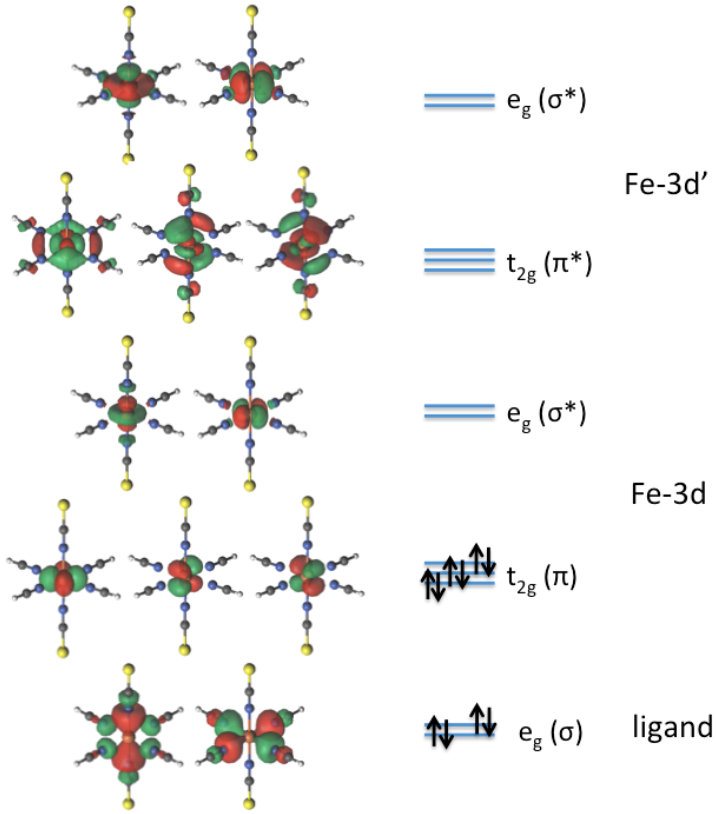

Figure 2.2: The selection of active spaces for CASSCF/CASPT2[10,12] calculations in the $Fe(NCH)_4(NCS)_2$ complex.

Chapter 3

Results and Discussion

3.1 Results of $Fe(NCH)_4(NCS)_2$

3.1.1 Relative stability of the high spin state

In Figure 3.1, the different electronic configurations of the high spin state were explored to find the lowest configuration and to see if the excited states was Jahn-Teller active. The Jahn-Teller distorted structure was checked by lowering the symmetry from D_{4h} to D_{2h}. The PBE0 results for the relative stability of different configurations of the high spin state are shown in Table 3.1.

The energies of $^5B_{2g}$ (D_{4h}) and $^5B_{1g}$ (D_{2h}) states are identical. As expected, the Jahn-Teller effect does not influence the geometry of the lowest HS state. The $^5B_{2g}$ and $^5B_{3g}$ states of D_{2h} have a lower energy than ^5E_g state of D_{4h}, but the energy-lowering is not sufficient to make one of them the ground state. The structure of the HS state does not distort to lower symmetry. For further calculations, the $^5B_{2g}$ (D_{4h}) was used for the HS state structure.

Table 3.1 PBE0 results of the relative stability of the different electronic configurations of the high spin state in kcal/mol with respect to $^5B_{1g}$ state (D_{2h}).

	Energy		Energy
D_{4h}		D_{2h}	
$^5B_{2g}$	0.00	$^5B_{1g}$	0.00
^5E_g	32.63	$^5B_{2g}$	10.00
		$^5B_{3g}$	10.00

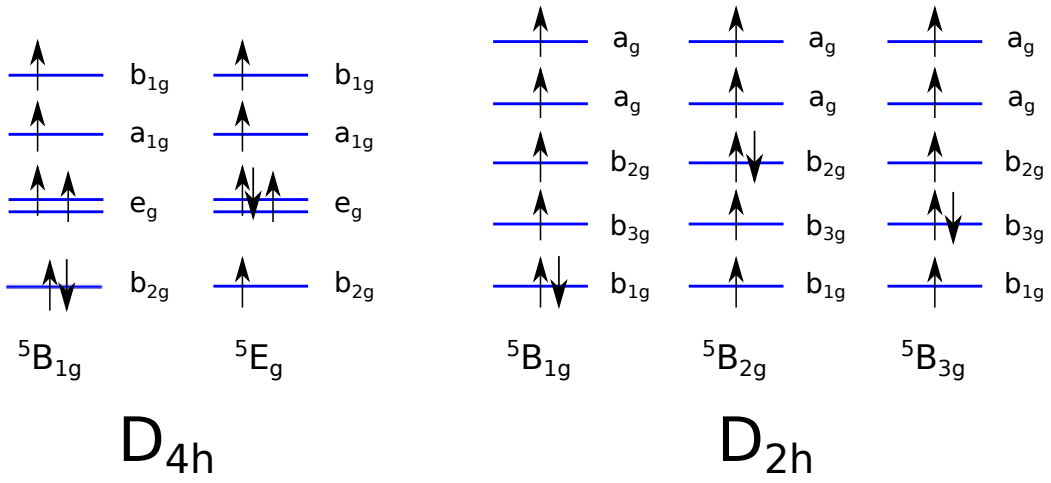

Figure 3.1: The different electronic configurations of the quintet states.

3.1.2 The optimized structure

The optimized geometries at PBE0 level were compared with CASPT2 optimized metal-ligand distances (CASPT2/PBE0), as well as fully optimized geometries at the CASPT2 level (Table 3.2). The PBE0 geometries for the ligands are in good agreement with the CASPT2 geometries (except N-C distances), while the metal-ligand distances are quite different. The metal-ligand distances differ by up to 0.058 Å while the ligand distances (N-C) differ by up to 0.019 Å. The improved structures, the optimized metal-ligand distances from a quadratic fitting (CASPT2/PBE0), are really in good agreement with fully optimized geometries at CASPT2 level. The metal-ligand distances differ by up to 0.005 Å. The CASPT2/PBE0 optimization can be used as an inexpensive method to optimize metal-ligand distances.

In the low spin state, the Fe-NCS distance is slightly longer than the Fe-NCH distance. The difference between them is only 0.02 Å. The situation is different in the quintet state. When the electrons go from the non-bonding $t_{2g}(O_h)$ orbital to the antibonding $e_g(O_h)$ orbital, from LS to HS, the electronic repulsion strongly increases while occupying the antibonding e_g. As the consequence of increasing the electronic repulsion, the lengthening of the Fe-N bond lengths occurs. The Fe-NCH distance is longer than the Fe-NCS distance by about 0.25 Å. The Fe-NCH changes 0.35 Å from the LS to the HS structure while the F-NCS changes 0.11 Å. The change in metal-ligand bond lengths between two states is considered as driving force for the spin crossover processes [3, 47].

3.1.3 CASPT2 energies

In Table 3.3, the energy difference between HS and LS is shown for the three different geometries and based on four different actives spaces. All methods show that the high spin state is lower in energy than the low spin state. The energy difference between

Table 3.2 Bond distances (in Å) for the optimized geometries at different levels of theory

Bond	PBE0	CASPT2/ PBE0 Basis I	CASPT2/ PBE0 Basis II	Fully CASPT2 Basis II	PBE0	CASPT2/ PBE0 Basis I	CASPT2/ PBE0 Basis II	Fully CASPT2 Basis II
Low Spin					**High Spin**			
-NCH								
Fe-N	1.921	1.870	1.863	1.863	2.266	2.226	2.211	2.216
N-C	1.140	1.140	1.140	1.159	1.142	1.142	1.142	1.149
C-H	1.068	1.068	1.068	1.067	1.069	1.069	1.069	1.067
-NCS								
Fe-N	1.930	1.885	1.883	1.883	1.991	1.990	1.992	1.993
N-C	1.172	1.172	1.172	1.186	1.178	1.178	1.178	1.183
C-S	1.612	1.612	1.612	1.615	1.602	1.603	1.603	1.610

HS and LS is affected by the geometry significantly. The energy difference at PBE0 optimized structure is about 1000 cm^{-1} larger than the energy difference at the fully optimized CASPT2 structure. The energy differences are improved by about 800 cm^{-1} with CASPT2/PBE0 structure.

The information about the importance and sources of (non-dynamical) correlation effects is obtained by gradually increasing the active space. The CAS[10,10] is considered as minimum active space to capture the essential correlation effects. In CAS[10,10], the reference wave function is built by distributing ten electrons over two ligands orbitals with e_g symmetry and three non-bonding orbitals of iron 3d with t_{2g} symmetry. The virtual orbitals with predominant iron d character, the anti-bonding e_g orbitals and the t'_{2g} orbitals of iron are included in the active space. The t'_{2g} shell is included in order to describe the double-shell effect, i.e. radial correlation effects within the iron 3d shell [35].

In CAS[10,12], two anti-bonding orbitals of e'_g symmetry are included to fully describe the double-shell effect on HS state. The state average (SA) and state specific (SS) CAS[10,12] methods were performed. In the SA method, the LS CASSCF wave function is obtained by averaging 94% weighted to singlet ground state and 6% weighted to three low-lying singlet excited states while for HS CASSCF wave function was obtained by 100% weighted to the quintet ground state. The SS CAS[10,12] method is constructed of CAS[10,10] for LS state and CAS[10,12] for HS state. The SA CASPT2[10,12] result has larger Δ_{HL} than the SS CASPT2[10,12] result, due to averaging. The LS state obtained from SA CAS[10,12] goes a little bit high in energy. We consider the SS CASPT2[10,12] is sufficient in order to get reasonable Δ_{HL}. For the LS state, we kept CAS[10,10]. As consequence of having no electrons in the anti-bonding e_g orbitals, it is not necessary to include e'_g shell in the active space. The possible unbalance in the description with this choice of CASSCF wave functions is corrected by including dynamical correlation with

Table 3.3 The energy difference of high spin and low spin states in cm^{-1} with basis II

optimized geometry	DFT PBE0	CASPT2 (10,10)	SA CASPT2 (10,12)[a]	CASPT2 (10,12)[b]	CASPT2 (10,13)	CASPT2 (10,15)
PBE0	-5751	-6662	-	-4205	-6304	-
CASPT2/PBE0		-5850	-	-3379	-	-
Fully CASPT2		-5671	-4248	-3200	-	-2910

[a]LS: 94% weighted to singlet ground state and 6% weighted to three singlet excited states, HS: 100% weighted to quintet ground state

[b]CASPT2[10,12] for HS spin state and CASPT2[10,10] for LS spin state

CASPT2 procedure.

Increasing the active space from CAS[10,10] to CAS[10,12] for the HS state does lead to a significant gain in non-dynamical correlation effects, of about 2300 cm^{-1}. This improvement is due to having a double shell also for the e'_g orbitals in the active space. Adding extra Π^* ligands orbitals to the CAS[10,10] and CAS[10,12] does not change the relative energies significantly, only about 300 cm^{-1}. The computational cost of adding extra three orbitals to the active space is not justified by the improvement of Δ_{HL}. In conclusions, the CAS[10,12] is considered as an adequate method.

3.1.4 Basis set dependency

To investigate the basis sets effects on Δ_{HL}, three different basis sets were used in the CASPT2 calculations(Table 3.4). The investigations were performed using CASPT2[10,12] procedure on the fully CASPT2 structure.

In this work, the smallest basis set (basis I) was still fairly extensive, quintuple-zeta with up to g-type polarization functions on the metal and triple-zeta with d-type polarization functions on the ligand donor atoms. Adding polarization functions up to h-type on the metal and f-type on the ligand donor atoms (basis II) improved Δ_{HL} significantly, with about 1000 cm^{-1}. Apparently higher polarization functions on metal and ligands are needed in order to get better the Δ_{HL}.

In Ref. [35], the basis II was considered as an adequate basis set to calculate Δ_{HL}. To check the adequacy, the basis II was compared to an extremely large basis set (basis III), octuple-zeta with up to h-type polarization functions on metal and the ligand donor. The basis III does not give significant improvement on Δ_{HL}, about 300 cm^{-1}, which is still within chemical accuracy 1 kcal/mol (350 cm^{-1}). The basis set II is considered as a adequate basis set for further study, it compromises computational cost and accuracy.

Table 3.4 The CASPT2 energy difference of high spin and low spin with different basis sets (in cm^{-1})

Basis set	ANO-rcc (basis I)	ANO-rcc (basis II)	ANO-rcc (basis III)
CASPT2[10,12] [a]	-4128	-3200	-2953

[a]CASPT2[10,12] for HS spin state and CASPT2[10,10] for LS spin state

3.1.5 Potential energy profile

The potential energy profile was investigated in order to get an estimate of the activation energy for the spin transition. The potential energy profile of Fe(NCS)$_2$(NCH)$_4$ is obtained by doing linear interpolation for all coordinates between LS structure to HS structure (Figure 3.2). The symmetric vibrational mode was chosen as a reaction path [48]. The pseudo-octahedral Fe(II) complexes are known to exhibit a rather weak ligand-field splitting, which leads to the presence of two energetically nearly degenerate states [13]. It was found that this complex has HS ground state. It might be that all six ligands cause a too weak field. In a previous study, Domingo and coworkers [4] have demonstrated that the NCH ligand causes a weaker field than the NCS ligand. They have demonstrated that the ligands, H_2O <NH_3 <NCH <NCS <CO <PH_3, form a spectrochemical series from weak to strong field.

As consequence of the fairly weak field, the energy gap between the non-bonding t_{2g} and the anti-bonding e_g orbitals, Δ_0, is small. In the situation when the Δ_0 is smaller than the spin-pairing energy, the HS state is favored. The two states do not have the same equilibrium distances. For the Fe(NCS)$_2$(NCH)$_4$, this complex reaches the equilibrium distance for the LS state at 1.86 Å for Fe-NCH and 1.88 Å for Fe-NCS. For HS state, the equilibrium distance is reached at 2.22 Å for Fe-NCH and 1.99 Å for Fe-NCS. The displacement for the -NCH ligand is larger than that for the -NCS ligand because of the smaller mass of the ligand. The metal-ligand averaged distance (2.14 Å) in the HS state is close to the distance found when all ligand-metal distances are forced to be equal (2.12 Å) as shown in Ref. [4]. The activation energy to go from the LS state to the HS state is about 1200 cm^{-1}, while the reverse process has an activation energy of about 4400 cm^{-1}.

3.2 Results of Fe(bpy)$_2$(NCS)$_2$

After validation of the method on the model system, Fe(NCH)$_4$(NCS)$_2$, the proposed method was used for the real system, Fe(bpy)$_2$(NCS)$_2$, which has C_2 symmetry. CASPT2[10,12] was used for calculating the HS-LS energy difference. The CASPT2/PBE0 procedure was used for the geometry optimization.

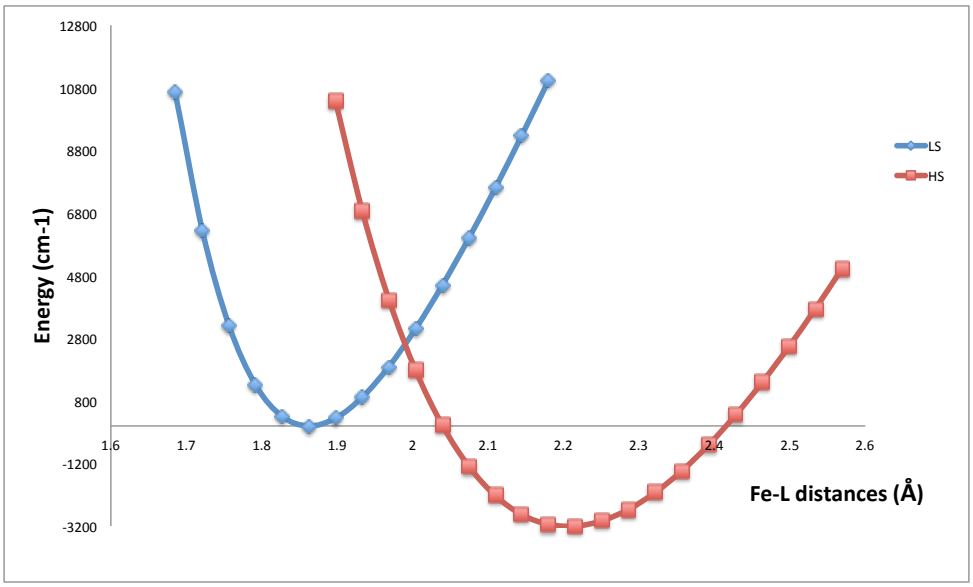

Figure 3.2: Potential energy profile of $Fe(NCS)_2(NCH)_4$.

3.2.1 Relative stability of the high spin state

Three different electronic configurations for the HS state in the C_2 symmetry were explored to find the lowest electronic configuration (Figure 3.3). Two ^5A states configurations are degenerate. The ^5B state has the lowest energy (Figure 3.3). The lowering in energy from ^5A to ^5B state is 0.13 kcal/mol (6 meV). For further calculations, the ^5B state (C_2) geometry was used as the HS state structure.

3.2.2 The optimized structure

The optimized structure at PBE0 level, CASPT2/PBE0, and the experimental structure are shown in Table 3.5. The PBE0 optimized structures are in good agreement with experimental data [2]. The metal-ligand distances optimized with PBE0 differ from the experimental data by up to 0.009 Å for the LS geometry and 0.12 Å for the HS geometry. The CASPT2/PBE0 optimized structure tends to have shorter distances than the PBE0 optimized structure. The metal-ligand distances optimized with the CASPT2/PBE0 procedure deviate c.a. 0.1 Å for HS and LS state from the experiment data.

The Fe-N(NCS) bond-lengths are more or less the same as the Fe-N(bpy) bond-lengths in the LS state, about 1.9 Å. The metal-ligand Fe-N bond-lengths become longer in the HS state. In HS state, the agreement between the PBE0 and M-L CASPT2 results is very reasonable, but the deviation from the experimental values is rather large. The bond-lengths difference between HS and LS state is called Δr_{HL}. The experimental Δr_{HL} for Fe-N(NCS) is 0.1 Å, while Δr_{HL} for Fe-N(bpy) is 0.2 Å [2]. The PBE0 method gives Δr_{HL} in good agreement with experimental data, while the CASPT2/PBE0 procedure

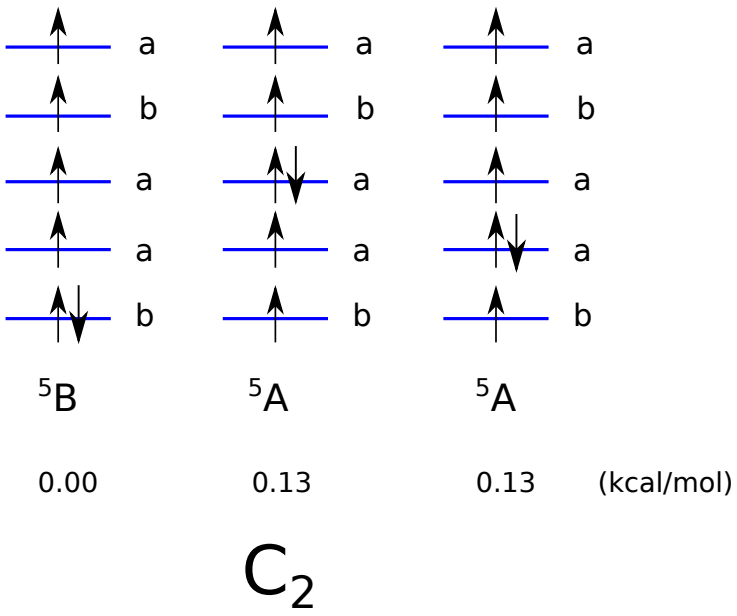

Figure 3.3: The different electronic configurations of the quintet states and PBE0 relative energy in kcal/mol with respect to ^{5}B state.

Table 3.5 Bond distances (in Å) for the optimized geometries at different levels of theory and compared with experiment (Ref. [2])

Bond	PBE0	CASPT2/ PBE0 Basis I	Exp.	PBE0	CASPT2/ PBE0 Basis I	Exp.
Low Spin				**High Spin**		
Fe-NCS	1.941	1.888	1.945(3)	2.026	2.017	2.053(5)
Fe-N(bpy)(1)	1.973	1.897	1.964(2)	2.233	2.229	2.181(4)
Fe-N(bpy)(2)	1.979	1.870	1.969(3)	2.289	2.272	2.166(4)

Table 3.6 The energy difference of high spin and low spin states in cm^{-1} with basis I

geometry	DFT PBE0	CASPT2 (10,12)[b]	Exp.[a]
PBE0	-3480	-1111	
CASPT2/PBE0	-5630	573	
Exp.			844 ± 42

[a]reference [17]
[b]CASPT2[10,12] for HS spin state and CASPT2[10,10] for LS spin state

overestimates the Δr_{HL}.

3.2.3 The HS-LS energy difference

The energy difference between HS and LS states, Δ_{HL}, is shown in Table 3.6. The geometry affects Δ_{HL} significantly. The PBE0 structure gives a qualitatively and quantitatively wrong value for Δ_{HL}. The PBE0 method gives HS ground state, which is not in agreement with experimental ground state. The HS-LS energy differences at the PBE0 level and the CASPT2 level, both are calculated at the PBE0 optimized geometry are -3480 and -1110 cm^{-1}, respectively. Evaluating the Δ_{HL} using the CASPT2/PBE0 optimized structure improves this energy difference significantly. The HS-LS energy difference at CASPT2 level with the CASPT2/PBE0 optimized structure is 573 cm^{-1} which is really in good agreement with experimental Δ_{HL} of 844 ± 42 cm^{-1} [17].

Chapter 4

Conclusions

4.1 Summary

Multiconfigurational second-order perturbation theory (CASPT2) has been applied to study the structural properties that change during SCO processes, the relative energy difference between HS and LS states, and the potential energy profiles. The aim of investigation the hypothetical model, $Fe(NCS)_2(NCH)_4$, is to establish an appropriate computational procedure (geometries, active space and basis set) to study SCO systems. The gradually increasing active spaces and basis sets lead to an increasing account of the important source of non-dynamical correlation effects, leading to a better description of the energy difference between HS and LS states.

Based on this investigation, the CASPT2[10,12] approach turns out to be sufficient to study the structural properties, the relative energy difference, and potential energy profiles. The CASPT2 [10,12] approach is a compromise between computational cost and accuracy. The quintuple-zeta basis on Fe with polarization functions up to h-type and triple-zeta basis on the donor ligand atoms with polarization functions up to f-type on the ligand donor atoms, is necessary in order to obtain an accurate HS-LS energy difference. The CASPT2/PBE0 method is recommended as a relatively inexpensive alternative to obtain geometries close to the fully CASPT2 geometry.

4.2 Outlook

Further work is to investigate some low-lying excited states in order to understand why the $Fe(bpy)_2(NCS)_2$ complex is not an active-LIESST complex.

Acknowledgements

First of all, I would like to thank to my supervisor Prof. Dr. Ria Broer for giving me the opportunity to follow the European Master in Theoretical Chemistry and Computational Modelling (EMTCCM 2010-2012) and her guidance during my master study. She taught me how to become a scientist. I would also like to thank Prof. Dr. Kristine Pierloot, Dr. Steven Vancoillie, and Dr. Remco W. A. Havenith for supervising me. I am really proud that I became your student. You are really good scientists.

I am grateful to Professor Philipp Gütlich, Coen de Graaf, Hélène Bolvin, and Andrii Rudavskyi for useful discussion about spin crossover and methods. I would also like to address my gratitude to Professor Roland Lindh and Per-Åke Malmqvist for their help and initial investigation during ^{7th}MOLCAS workshop in Uppsala, Sweden. I am indebted to Dr. Rémi Maurice and Quan Manh Phung for reading and correcting my thesis. Thank is also to Hilde de Gier for nice discussions and help. Last but not least, I would like to thank the Erasmus Mundus Program of the European Union (FPA 2010-0147) for the financial support.

References

[1] Philipp Gütlich, Yann Garcia, and Harold A. Goodwin. Spin crossover phenomena in Fe(II) complexes. *Chem. Soc. Rev.*, 29(6):419–427, 2000.

[2] Michiko Konno and Mami Mikami-Kido. Temperature- or pressure-induced structure changes of a spin crossover Fe(II) complex; (Fe(bpy)2(NCS)2). *Bull. Chem. Soc. Jpn.*, 64(2):339–345, 1991.

[3] Andreas Hauser. Ligand field theoretical considerations. In P. Gütlich and H.A. Goodwin, editors, *Spin Crossover in Transition Metal Compounds I*, volume 233 of *Topics in Current Chemistry*, pages 49–58. Springer Berlin, Heidelberg, 2004.

[4] Alex Domingo, Maria Ángels Carvajal, and Coen de Graaf. Spin crossover in Fe(II) complexes: An ab initio study of ligand σ donation. *Int. J. Quantum Chem.*, 110(2):331–337, February 2010.

[5] Philipp Gütlich, Harold A. Goodwin, P. Gütlich, and H.A. Goodwin. Spin crossover in transition metal compounds i. volume 233 of *Topics in Current Chemistry*, pages 1–47. Springer Berlin, Heidelberg, 2004.

[6] Ana B. Gaspar, Vadim Ksenofontov, Maksym Seredyuk, and Philipp Gütlich. Multifunctionality in spin crossover materials. *Coord. Chem. Rev.*, 249(23):2661–2676, December 2005.

[7] L. Cambi and L. Szegö. Über die magnetische susceptibilität der komplexen verbindungen. *Berichte der deutschen chemischen Gesellschaft (A and B Series)*, 64(10):2591–2598, April 2008.

[8] Sason Shaik, Devesh Kumar, Samuel P de Visser, Ahmet Altun, and Walter Thiel. Theoretical perspective on the structure and mechanism of cytochrome p450 enzymes. *ChemInform*, 36(37):no–no, September 2005.

[9] W. Robert Scheidt and Christopher A. Reed. Spin-state/stereochemical relationships in iron porphyrins: implications for the hemoproteins. *Chem. Rev.*, 81(6):543–555, 1981.

[10] M. F. Perutz, G. Fermi, B. Luisi, B. Shaanan, and R. C. Liddington. Stereochemistry of cooperative mechanisms in hemoglobin. *Acc. Chem. Res.*, 20(9):309–321, 1987.

[11] Md. Ehesan Ali, Biplab Sanyal, and Peter M. Oppeneer. Electronic structure, Spin-States, and Spin-Crossover reaction of Heme-Related Fe-Porphyrins: a theoretical perspective. *J. Phys. Chem. B*, 116(20):5849–5859, 2012.

[12] Mikaël Kepenekian, Boris Le Guennic, and Vincent Robert. Magnetic bistability: From microscopic to macroscopic understandings of hysteretic behavior using ab initio calculations. *Phys. Rev. B*, 79(9):094428, March 2009.

[13] David N. Bowman and Elena Jakubikova. Low-Spin versus High-Spin ground state in Pseudo-Octahedral iron complexes. *Inorg. Chem.*, 51(11):6011–6019, 2012.

[14] Hélène Bolvin. d-d spectrum and High-Spin/Low-Spin competition in d^6 octahedral coordination compounds:*ab Initio* study of potential energy curves. *J. Phys. Chem. A*, 102(38):7525–7534, 1998.

[15] Philipp Gütlich, Andreas Hauser, and Hartmut Spiering. Thermal and optical switching of Iron(II) complexes. *Angewandte Chemie International Edition in English*, 33(20):2024–2054, December 2003.

[16] Duward Shriver, Peter Atkins, Tina Overton, and Jonathan Rourke. *Inorganic Chemistry*. W. H. Freeman, December 2009.

[17] S.K. Kulshreshtha and R.M. Iyer. Nature of the high-spin ($^5t_2$)-low-spin ($^1a_1$) transition in [Fe(bipy)2(NCS)2]. *Chem. Phys. Lett.*, 108(5):501–504, July 1984.

[18] Coen de Graaf and Carmen Sousa. Study of the LightInduced spin crossover process of the [FeII(bpy)3]2+ complex. *Chem. Eur. J.*, 16(15):4550–4556, April 2010.

[19] Per-Åke Malmqvist, Kristine Pierloot, Abdul Rehaman Moughal Shahi, Christopher J Cramer, and Laura Gagliardi. The restricted active space followed by second-order perturbation theory method: Theory and application to the study of CuO_2 and Cu_2O_2 systems. *J. Chem. Phys*, 128(20):204109–204109–10, May 2008.

[20] Valera Veryazov, Per-Åke Malmqvist, and Björn O. Roos. How to select active space for multiconfigurational quantum chemistry? *Int. J. Quantum Chem.*, 111(13):3329–3338, April 2011.

[21] Daniel Roca-Sanjuán, Francesco Aquilante, and Roland Lindh. Multiconfiguration second-order perturbation theory approach to strong electron correlation in chemistry and photochemistry. *Wiley Interdisciplinary Reviews: Computational Molecular Science*, 00:1–19, 2011.

[22] B. O. Roos. Multiconfigurational second order perturbation theory (CASPT2). In *European Summerschool in Quantum Chemistry 2009*, number II, pages 301–312. Lund University, Lund, Sweden, Per-Olof widmark edition, 2009.

[23] Sérgio Filipe Sousa, Pedro Alexandrino Fernandes, and Maria João Ramos. General performance of density functionals. *J. Phys. Chem. A*, 111(42):10439–10452, 2007.

[24] Jianmin Tao and John P. Perdew. Test of a nonempirical density functional: Short-range part of the van der waals interaction in rare-gas dimers. *J. Chem. Phys*, 122(11):114102–114102–7, March 2005.

[25] David C. Patton and Mark R. Pederson. Application of the generalized-gradient approximation to rare-gas dimers. *Phys. Rev. A*, 56(4):R2495–R2498, October 1997.

[26] E. Engel and S. H. Vosko. Fourth-order gradient corrections to the exchange-only energy functional: Importance of a ∇^2 contributions. *Phys. Rev. B*, 50(15):10498–10505, October 1994.

[27] Philipp Dufek, Peter Blaha, and Karlheinz Schwarz. Applications of engel and vosko's generalized gradient approximation in solids. *Phys. Rev. B*, 50(11):7279–7283, 1994.

[28] Alexander Khein, D. J. Singh, and C. J. Umrigar. All-electron study of gradient corrections to the local-density functional in metallic systems. *Phys. Rev. B*, 51(7):4105–4109, February 1995.

[29] Carlo Adamo and Vincenzo Barone. Toward reliable density functional methods without adjustable parameters: The PBE0 model. *J. Chem. Phys*, 110(13):6158–6170, April 1999.

[30] Axel D. Becke. Density functional thermochemistry. IV. a new dynamical correlation functional and implications for exactexchange mixing. *J. Chem. Phys*, 104(3):1040–1046, January 1996.

[31] A. D. Becke. Density-functional exchange-energy approximation with correct asymptotic behavior. *Phys. Rev. A*, 38(6):3098–3100, 1988.

[32] Chengteh Lee, Weitao Yang, and Robert G. Parr. Development of the Colle-Salvetti correlation-energy formula into a functional of the electron density. *Phys. Rev. B*, 37(2):785–789, January 1988.

[33] Patrick W. M. Jacobs. *Group Theory With Applications In Chemical Physics*. Cambridge University Press, October 2005.

[34] TURBOMOLE v6.3 2011, a development of university of karlsruhe and forschungszentrum karlsruhe GmbH, 1989-2007, TURBOMOLE GmbH, since 2007; available from http://www.turbomole.com.

[35] Kristine Pierloot and Steven Vancoillie. Relative energy of the high- and low- spin states of [Fe(H2O)6]2+, [Fe(NH3)6]2+, and [Fe(bpy)3]2+: CASPT2 versus density functional theory. *J. Chem. Phys*, 125(12):124303–124303–9, September 2006.

[36] Gunnar Karlström, Roland Lindh, Per-Åke Malmqvist, Björn O Roos, Ulf Ryde, Valera Veryazov, Per-Olof Widmark, Maurizio Cossi, Bernd Schimmelpfennig, Pavel Neogrady, and Luis Seijo. MOLCAS: a program package for computational chemistry. *Computational Materials Science*, 28(2):222–239, October 2003.

[37] Francesco Aquilante, Luca De Vico, Nicolas Ferré, Giovanni Ghigo, Per-Åke Malmqvist, Pavel Neogrády, Thomas Bondo Pedersen, Michal Pitoňák, Markus Reiher, Björn O. Roos, Luis Serrano-Andrés, Miroslav Urban, Valera Veryazov, and Roland Lindh. MOLCAS 7: The next generation. *J. Comput. Chem.*, 31(1):224–247, January 2010.

[38] Marvin Douglas and Norman M Kroll. Quantum electrodynamical corrections to the fine structure of helium. *Annals of Physics*, 82(1):89–155, 1974.

[39] Bernd A. Hess. Relativistic electronic-structure calculations employing a two-component no-pair formalism with external-field projection operators. *Phys. Rev. A.*, 33(6):3742–3748, June 1986.

[40] Björn O. Roos, Roland Lindh, Per-Åke Malmqvist, Valera Veryazov, and Per-Olof Widmark. New relativistic ANO basis sets for transition metal atoms. *J. Phys. Chem. A*, 109(29):6575–6579, 2005.

[41] Kristine Pierloot. The CASPT2 method in inorganic electronic spectroscopy: from ionic transition metal to covalent actinide complexes. *Mol. Phys.*, 101(13):2083–2094, 2003.

[42] Kerstin Andersson and Björn O. Roos. Excitation energies in the nickel atom studied with the complete active space SCF method and second-order perturbation theory. *Chem. Phys. Lett.*, 191(6):507–514, April 1992.

[43] C. de Graaf, R. Broer, and W.C. Nieuwpoort. Electron correlation effects on the d-d excitations in NiO. *Chemical Physics*, 208(1):35–43, July 1996.

[44] Belén Ordejóln, Coen de Graaf, and Carmen Sousa. Light-Induced Excited-State spin trapping in Tetrazole-Based spin crossover systems. *J. Am. Chem. Soc.*, 130(42):13961–13968, 2008.

[45] Niclas Forsberg and Per-Åke Malmqvist. Multiconfiguration perturbation theory with imaginary level shift. *Chem. Phys. Lett.*, 274(13):196–204, August 1997.

[46] Giovanni Ghigo, Björn O. Roos, and Per-Åke Malmqvist. A modified definition of the zeroth-order hamiltonian in multiconfigurational perturbation theory (CASPT2). *Chem. Phys. Lett.*, 396(13):142–149, September 2004.

[47] A. H. Ewald, R. L. Martin, I. G. Ross, and A. H. White. Anomalous Behaviour at the $^6A_1$-$^2T_2$ Crossover in Iron (III) Complexes. *Proceedings of the Royal Society of London. Series A. Mathematical and Physical Sciences*, 280(1381):235–257, July 1964.

[48] Takeshi Tayagaki and Koichiro Tanaka. Photoinduced phase transition to a new macroscopic Spin-Crossover-Complex phase. *Phys. Rev. Lett.*, 86(13):2886–2889, March 2001.